Semilunar Granule Cells Maintain Distinct Dendritic Morphology and Inhibition through Postnatal Development and Receive Heightened Inhibition in Adolescence

Akshay Gupta[1,3], Deepak Subramanian[1,3], Archana Proddutur[1,3], Yun-Juan Chang[2], Jenieve Guevarra[1], Yash Shah[1], Fatima S. Elgammal[1], and Vijayalakshmi Santhakumar[1,3]

[1]Department of Pharmacology, Physiology and Neuroscience, [2]Office of Advance Research Computing, Rutgers New Jersey Medical School, Newark, New Jersey 07103, [3]Department of Molecular, Cell and Systems Biology, University of California Riverside, Riverside, California 92521.

Short Title SGCs during postnatal development

Word count for Abstract: 199

Full Text Character count: 6773 words Number of pages: 39 Number of figures: 7

Number of Supplementary Figures: 5 Color figures: 2 Number of Tables: 0

Number of Supplementary Tables: 6

Author Contributions: AG, DS, JG, and AP performed experiments; AG, D.S, Y-JC, and YS analyzed data; AG, DS, FSE, and VS interpreted results of experiments; AG, AP, and DS prepared figures; AG and VS conceived of and designed research; AG, DS, and VS drafted manuscript.

Correspondence:

Vijayalakshmi Santhakumar, PhD
Department of Molecular, Cell and Systems Biology
University of California, Riverside
3401 Watkins Drive (Rm 1308 Spieth Hall) Riverside, CA 92521
E-mail: vijayas@ucr.edu

Abstract

Semilunar granule cells (SGCs) have been proposed as a morpho-functionally distinct class of hippocampal dentate projection neurons contributing to feedback inhibition and memory processing in juvenile rats. However, whether SGCs retain their unique structural and inhibitory characteristics through postnatal development remains unresolved. Focusing on postnatal days 11-13, 28-42, and >120, corresponding with human infancy, adolescence, and adulthood, we examined whether SGCs differ from granule cells (GCs) in somatodendritic morphology and inhibitory regulation. Unsupervised cluster analysis confirmed that morphological features distinguish SGCs from GCs irrespective of animal age. SGCs maintain higher spontaneous inhibitory postsynaptic current (sIPSC) frequency than GCs from infancy through adulthood. While sIPSC frequency peaked during adolescence, and amplitude declined progressively with age in both cell types, sIPSC frequency in SGCs was particularly enhanced during adolescence. Like GABAergic synaptic inputs, extrasynaptic GABA current amplitude in SGCs peaked in adolescence and was greater than in GCs. Consistent with the developmental profile of SGC synaptic and extrasynaptic GABA currents, perforant-path evoked dentate population responses *in vivo* showed greater paired-pulse depression during adolescence. These findings highlight the distinct morphology and inhibitory regulation of SGCs through development and suggest that the particularly heightened inhibition of SGCs may shape dentate output during adolescence.

Keywords: inhibition, GABA, dentate gyrus, extrasynaptic, development, granule cell, semilunar granule cell

The dentate gyrus, the primary gateway for cortical inputs to the hippocampus, plays a unique role in memory processing as a center for sparse coding mediated, in large part, by strong inhibitory filtering of activity (Dengler CG and DA Coulter 2016). The classical dentate projection neurons, granule cells (GCs), which number in over a million in the rat brain, rest at more hyperpolarized potentials than most hippocampal neurons, receive powerful feedback inhibition, and project strong "detonator" synapses to CA3 enabling sparse yet reliable transmission (Engel D and P Jonas 2005; Dengler CG and DA Coulter 2016). Recent characterization of semilunar granule cells (SGCs), a dentate cell-type originally identified by Ramón y Cajal S (1953), has revealed a second class of dentate projection neurons that are located in the inner molecular layer (IML), has distinctive somato-dendritic structure, persistent firing, and robust inhibition (Williams PA et al. 2007; Larimer P and BW Strowbridge 2010; Gupta A et al. 2012). While SGCs have been physiologically defined in rat (Williams PA *et al.* 2007; Gupta A *et al.* 2012), cells with dendritic morphology consistent with SGCs have been observed in primates (Duffy CJ and P Rakic 1983; Seress L and M Frotscher 1990). Additionally, physiological recordings from cells with morphological features of SGCs have been performed in mouse and rabbit (Sancho-Bielsa FJ et al. 2012; Save L et al. 2018), indicating their presence across mammalian species. Due to their unique persistent firing in response to inputs, SGCs have been proposed to play a crucial role in regulating GC feedback inhibition, sparse coding of inputs, and pattern separation (Larimer P and BW Strowbridge 2010; Walker MC et al. 2010). Since SGCs lack a distinct neurochemical marker, morphological characteristics are currently the primary approach to identify SGCs. However, the limited literature on SGC morphology and synaptic inputs have impeded further analysis of the role of SGCs in the dentate circuit.

Developmentally, both SGCs and GCs express the homeodomain transcription factor Prox1 (Gupta A *et al.* 2012) and derive from the same neural precursor pool, although SGCs differentiate in a more restricted embryonic phase, demonstrating a common lineage between SGCs and GCs (Kerloch T et al. 2018; Save L *et al.* 2018). Based on the embryonic developmental analysis, SGCs are estimated at 3% of the neurons generated from the dentate neurogenic pool from which GCs derive (Save L *et al.* 2018). Like GCs, SGCs have dendrites in the dentate molecular layer, and axons projecting to CA3. However, they can be distinguished from GCs based on their expansive dendritic span, large semi-lunar somata in the inner molecular layer (IML), and frequent presence of IML axon collaterals (Williams PA *et al.* 2007; Gupta A *et al.* 2012). In earlier studies in rats, we defined SGCs on the basis of their wider dendritic angle (Gupta A *et al.* 2012), which was subsequently confirmed in mice (Save L *et al.* 2018). To date, morphometric analysis of SGCs has been limited to a narrow window of postnatal day (PD) 14-42 in rats, which is consistent with the neurological developmental state of human adolescence (Semple BD et al. 2013; Sengupta P 2013), or in an embryonically labeled subgroup of neurons in young adult mice (Save L *et al.* 2018). However, whether SGCs retain their distinct structural characteristics through postnatal development has not been examined. Recent studies have suggested layer specific differences in GC morphology (Kerloch T *et al.* 2018) and disease-related changes in GC dendritic features (von Campe G et al. 1997; Freiman TM et al. 2011; Llorens-Martin M et al. 2015). However, without knowing the specific structural features that distinguish GCs from SGCs, it is difficult to interpret whether reports on changes in GC morphology reflect inclusion of structurally distinct SGCs in the datasets. Moreover, the ability to reliably distinguish SGCs from GCs across animal age is a prerequisite to elucidating the unique role that SGCs play in dentate processing. Unsupervised analysis of dendritic

morphometric features is ideally suited to examine whether SGCs remain distinct from GCs through development and to elucidate the somato-dendritic features that specify the cell types.

Physiologically, SGCs show prolonged firing, reduced spike frequency adaptation, and lower input resistance than GCs (Williams PA *et al.* 2007; Gupta A *et al.* 2012; Save L *et al.* 2018). Unlike GCs, SGCs respond to perforant-path stimulation with persistent firing lasting several seconds, which correlates with periods of increased hilar activity termed “up-states” (Larimer P and BW Strowbridge 2010). SGCs have larger NMDA currents (Williams PA *et al.* 2007) than GCs, make synaptic contacts with hilar mossy cells and interneurons and have been proposed to drive granule cell feedback inhibition (Larimer P and BW Strowbridge 2010). Apart from excitation, we previously demonstrated that SGCs have greater synaptic and extrasynaptic GABA currents (Gupta A *et al.* 2012). Additionally, we identified that GCs and SGCs have diametrically opposite changes in synaptic and tonic GABA currents after brain injury suggesting that differences in inhibition which could contribute to distinct roles for SGCs and GCs in the dentate circuit. GCs undergo changes in both tonic and synaptic GABA currents during postnatal development (Hollrigel GS et al. 1998; Holter NI et al. 2010; Lee CY and HH Liou 2013). In parallel, studies on adult-born GCs labeled at specific time points show cell-age dependent maturation of GABA currents, ultimately reaching the levels similar to mature GCs in age-matched animals (Dieni CV et al. 2012; Li Y et al. 2012). Yet, whether inhibition in SGCs remains distinct from mature GCs through postnatal development is not known. While GCs show prolonged functional maturation (Yu EP et al. 2013), age-dependent changes in inhibitory regulation of SGCs remains to be tested. This study was conducted to explicitly test whether SGCs form a structurally distinct class of dentate neurons through specific postnatal developmental stages representing infancy (PD 11-13, prior to rodent eye opening), adolescence

(PD 28-42 days, period of corical maturation), and adult (> PD 120, cortical and sexual maturity) stages of development (Semple BD *et al.* 2013)and to identify the differences in steady-state inhibitory regulation of the two cell types through maturation of the dentate circuit.

Materials and Methods

Animals. All experiments were performed in accordance with IACUC protocols approved by Rutgers-NJMS, Newark, NJ, and the University of California at Riverside, CA and in keeping with the ARRIVE guidelines. The study included Wistar rats ranging in age from 11-13 days, 28-42 days, and 120-180 days designated as infancy, adolescence, and adulthood, respectively (Semple BD *et al.* 2013; Sengupta P 2013). Due to the potential effects of hormonal variation on GABA currents, slice recordings in rats from >28 days were restricted to males. A subset of recordings was derived from surgical or saline-injected controls for an independent study and was pooled with data from naïve rats from which they showed no statistical difference.

Slice Physiology. Rats were anesthetized with isoflurane and decapitated. Horizontal brain slices (300µm) were prepared in ice-cold sucrose artificial cerebrospinal fluid (sucrose-aCSF) containing the following (in mM): 85 NaCl, 75 sucrose, 24 $NaHCO_3$, 25 glucose, 4 $MgCl_2$, 2.5 KCl, 1.25 NaH_2PO_4, and 0.5 CaCl using a Leica VT1200S Vibratome. The slices were sagittally bisected and incubated at 32°C for 30 min in a submerged holding chamber containing an equal volume of sucrose-aCSF and recording aCSF, and subsequently were held at room temperature. The recording aCSF contained the following (in mM): 126 NaCl, 2.5 KCl, 2 $CaCl_2$, 2 $MgCl_2$, 1.25 NaH_2PO_4, 26 $NaHCO_3$, and 10 D-glucose. All solutions were saturated with 95% O_2 and 5% CO_2 and maintained at a pH of 7.4 for 1–6 h. Slices were transferred to a submerged recording chamber and perfused with oxygenated aCSF at 33°C. Whole-cell voltage-clamp recordings from neurons in the dentate granule cell layer (GCL) and inner molecular layer (IML) were performed using infrared differential interference contrast visualization techniques (Gupta A *et al.* 2012; Yu J et al. 2016) with a Nikon Eclipse FN-1 microscope, using a 40X, 0.80 NA water-immersion objective. Cells in the hilar-GCL border were not included in the study.

Recordings were obtained using MultiClamp 700B (Molecular Devices). Data were low-pass filtered at 3 kHz, digitized using DigiData 1440A, and acquired using pClamp10 at 10 kHz sampling frequency. Tonic and synaptic GABA currents were recorded in perfusing aCSF with no added GABA or GABA transporter antagonists in the recording solution (Gupta A *et al.* 2012; Yu J et al. 2013). Voltage-clamp recordings of inward GABA currents were obtained from a holding potential of -70 mV using microelectrodes (5–7 MΩ) containing (in mM): 125 CsCl, 5 NaCl, 10 HEPES, 2 $MgCl_2$, 0.1 EGTA, 2 Na-ATP, and 0.5 Na-GTP, titrated to a pH 7.25 with CsOH. Biocytin (0.2%) was included in the internal solution for post hoc cell identification, and the glutamate receptor antagonist kynurenic acid (3 mM KynA, Tocris Bioscience) was included in the external solution to isolate GABA currents. Among neurons recorded in the IML, only cells showing obtuse dendritic angles, presence of dendritic spines and axon projecting to the hilus (Gupta A *et al.* 2012) (Supplementary Figure 1) were included in the physiological analysis as putative SGCs. The somata of all GCs included in the analysis were located in the GCL. Recordings were discontinued if series resistance increased by >20%. Access resistance was not different between cell-types or between developmental groups. Following establishment of whole cell mode, baseline recordings were obtained for a minimum of five minutes in the presence of KynA prior to addition of GABA blockers. Recordings with excessive baseline fluctuations during the 3-5 minutes of recordings in KynA were discarded. All salts were purchased from Sigma-Aldrich (St. Louis, MO). Tonic GABA current, the steady-state current blocked by the $GABA_AR$ antagonist bicuculline methiodide (BMI, 100µM, Sigma-Aldrich) or gabazine (SR95531, 10 µM, Sigma-Aldrich), was measured as described previously (Gupta A *et al.* 2012; Yu J *et al.* 2013) using custom macros in IgorPro7.0 software (WaveMetrics). Following physiological recordings, slices were fixed in 0.2mM phosphate buffer containing 4%

paraformaldehyde at 4°C for 2 days. Biocytin staining was revealed using Alexa Fluor 594-conjugated streptavidin (Gupta A *et al.* 2012; Swietek B et al. 2016).

Morphometry and hierarchical cluster analysis. Sections were visualized and imaged using a Zeiss LSM 510 confocal microscope with a 20X, 0.5 NA objective. Cell reconstructions from confocal image stacks were performed using the directional kernels user-guided reconstruction algorithm in Neurolucida 360 (MBF Bioscience) followed by manual correction and validation in 3D. About 10-20 percent of each dendritic arbor was reconstructed manually. Neurolucida Explorer (MBF Biosciences) was used to extract non-nominal or non-ordinal somatodendritic morphological quantitative parameters (defined in Supplementary Tables 1 & 2) for use in statistical comparisons and hierarchical cluster analysis. A total of 42 projection neurons in which the dendritic arbors were fully reconstructed were analyzed. The software failed to quantify a subset of somatic parameters in 6 cells, and these cells were excluded from cluster analysis.

Data were tested for uniform distribution and each quantified variable was fit to the sum of two or more Gaussian functions and quality of fit determined using maximum likelihood analysis (MLA; v2test) to assess normal distribution of parameters within each cell type. Variables with a nonuniform distribution were used for subsequent cluster analysis. A total of 42 somato-dendritic parameters (Supplementary Tables 1 & 2) from 36 morphologically reconstructed neurons, including both features measured in Neurolucida Explorer from the 3D reconstructions and parameters measured manually in 2D rendering (Neurolucida 360, MicroBrightfield) were analyzed. Unsupervised clustering and principal component analyses of morphological properties were conducted within R version 3.5.0, using R package Cluster, FactoMineR, and factoextra by an investigator (Y-J C) blinded to cell types and age groups. Hierarchical clustering on the

selected principal components (PCs) was performed using Ward's Criterion with Euclidean distance to generate the dendrogram. The clustering partition was obtained from hierarchical clustering and improved with K-means method (Husson F et al. 2010). Silhouette width analysis was conducted to assess the validity of the clusters. Summary of morphological data and statistical analysis of morphometric parameters are presented in Supplementary Tables 3 and 4 respectively.

In Vivo Recordings: Animals were anesthetized using urethane (1.5g/kg, i.p.) and all recordings commenced 60-90 minutes post induction following confirmation of surgical anesthesia. Rats were secured in a stereotaxic frame and placed on a warming pad (Stoelting) to maintain optimal body temperature (37ºC) throughout the experiments. Platinum-Iridium Concentric bipolar stimulating electrodes (Microprobes) were used to stimulate medial perforant path (mPP) (AP: -4 mm, ML: +3mm, DV: -1.5mm from bregma for infant, ML: +4-4.2 mm, DV: -2mm from lambda for adolescent and adult). A single tungsten wire electrode (50µm diameter, California Wire Company) was positioned in the GCL guided by responses evoked by mPP stimulation (0.6mA, 150µs, 0.1Hz monophasic pulses; ISOflex, AMPI Israel). Coordinates used for dentate gyrus were, from bregma, AP: -2 mm, ML: +1.5 mm, DV: -2.2-2.5mm for infant, AP: -3.5 mm, ML: +2 mm, DV: -3mm for adolescent, and AP: -4 mm, ML: +2mm, DV: -3.5mm for adult animals. Final electrode positions were optimized for maximal evoked responses. Paired-pulse responses were evoked with a 20ms interval between pulses, averaged over 5 sweeps each (0.8-1mA, 150 µs, 0.1Hz, monophasic pulse). Current intensity was adjusted to levels that reliably produced population spike amplitude of 0.5mV or more. Adolescent and adult animals were transcardially perfused with 0.9% saline followed by 4% PFA and brains were extracted for histological confirmation of electrode track. Population spike amplitude was measured as detailed previously

(Neuberger EJ et al. 2017). Paired pulse ratio was calculated as the amplitude of population spike 2 /population spike1. Evoked responses were recorded and analyzed using LabChart 8.0 (AD Instruments). Data from animals in which the paired pulse ratio was >1, indicative of stimulating electrode in the lateral perforant path, were excluded.

Analysis and Statistics: Individual spontaneous inhibitory postsynaptic currents (sIPSCs) were detected using custom software in Igor-Pro7.0 (Gupta A *et al.* 2012). The investigator (AG) was blinded to cell type during analysis. Events were visualized, and any "noise" that spuriously met trigger specifications was rejected. Cumulative probability plots of sIPSC parameters were constructed using IgorPro by pooling an equal number of sIPSCs from each cell. Data are shown as mean±SEM (standard error of the mean) or median and interquartile range (IQR) where appropriate and presented in Supplementary Table 5. Kruskal-Wallis One Way Analysis of Variance on ranks was conducted on data which failed Shapiro Wilk test for normalcy or equal variance test. Two-way ANOVA (TW-ANOVA, SigmaPlot 12.3) and Bonferroni correction was used to test for statistical differences in tonic GABA currents. Summary data and details of the statistical tests used are included in Supplementary Tables 5 and 6 respectively. Sample sizes were not predetermined and conformed with those employed in the field. Significance was set to $p<0.05$, subject to appropriate Bonferroni correction. All custom macros for analysis and data sets will be made available on request upon publication of the study.

Results

Somato-dendritic characteristics distinguish SGCs from GCs throughout postnatal development.

To examine whether SGCs are structurally distinct from GCs throughout postnatal development, we undertook electrophysiological recordings from putative GCs and SGCs in the GCL and IML respectively, and filled cells with biocytin to recover their morphology. As illustrated by morphological reconstructions obtained from confocal images of biocytin filled neurons (Fig. 1), putative GCs exhibit compact molecular layer dendritic arbors while putative SGCs recorded in the IML consistently exhibited wider dendritic spread. These differences in dendritic spread are maintained throughout the three developmental stages tested. Additionally, the X-Y plane projection of the reconstructed neurons revealed the characteristic crescent shaped somata of SGCs. Figure 1 illustrates pseudocolor rendering of dendritic arbors with segments assigned on the basis of branch order in 3D reconstructions in Neurolucida 360. Color coding of the dendritic segments revealed that, in addition to differences in dendritic span, SGCs differed from GCs in the extent to which individual dendritic trees branched and the number of segments in different dendritic orders. Moreover, reconstructions suggest that GCs have a dense distribution of dendritic arbors in a compact volume while SGCs appear to have sparsely distributed dendrites in a larger volume. Thus, while 3D reconstructions demonstrate that SGCs maintain a *qualitative* pattern of dendritic arborization distinct from GCs at all postnatal ages examined, they reveal additional morphometric features which differ between cell types indicating a need for comprehensive unsupervised *quantitative* analysis of dendritic structure.

To determine if somato-dendritic parameters distinguish GCs from SGCs through development, we undertook the first unsupervised classification of dentate projection neurons on the basis of morphometry. Projection neurons were identified based on the presence of somata in the GCL or IML, axons with boutons entering the hilus and targeting CA3 (Supplementary Figure 1). Additionally, we find that both SGCs and GCs, have a high density of dendritic spines (Supplementary Figure 1), which we used as a criterion to distinguish projection neurons from local interneurons when the axon was not fully recovered. Morphometric parameters of the cells reconstructed in 3D were obtained from automated algorithms in Neurolucida 360 (definitions are included in Supplementary Tables 1 and 2). Principal Component Analysis (PCA) of 42 distinct morphometric parameters from 36 cells revealed a relatively high dimensional structure. The first three principal components (PCs) explained about 46% of the total variance in the data, while the first seven components retained over 85% of the variance (Supplementary Figure 2). PCA analysis of individual cells was projected on to the first three principal components and visualized in 3D representation, which suggested that the cells likely segregate by cell type (Fig. 2A) rather than developmental age of the rat (Fig. 2B).

PCA also revealed that the cells examined cluster more reliably with the same investigator assigned cell type (Fig. 2). A total of 36 dentate projection neurons (16 cells in infant, 10 cells in adolescent and 10 cells in adult), recovered based on the quantitative morphological features, were included in the clustering analysis. A hybrid approach of hierarchical clustering on principal components (HCPC) which helps in de-noising multidimensional dataset was adopted (Husson F *et al*. 2010). HCPC on the first seven components suggested four cluster partitioning groups (Fig 2C). Opening of the blinding revealed that the four putative clusters demonstrated a tendency for cells to cluster by putative cell-type. Cluster 1 included 11 cells classified as GCs

and one classified as an SGC by the investigator, Cluster 2 included five putative GCs and four putative SGCs. Consistent with the mixed population, cluster 2 had a silhouette score close to 0 indicating an unstable cluster. Clusters 3 and 4 consisted entirely of cell classified as SGC by the investigator (A.G). Overall, silhouette analysis supported the clustering of homogenous population but not the mixed population.

Identity of principal morphometric parameters that best represent the PCs

The PCs were examined further to identify the top five morphological variables which best represent the PC (cos2 $\geq$ 0.7) and the morphological features that contributed to PC variability (Supplementary Figure 2). The number of first, second, and third order dendritic segments (note: number of first order dendritic segments equals number of primary dendrites), number of second order nodes and soma width where the top five morphological features that best represented the PCs while dendritic area and volume contributed most to variability (Supplementary Figure 2). Although the dendritic span and angle, used by the experimenter for classification (Williams PA *et al*. 2007; Gupta A *et al*. 2012), contributed to the PC, morphology-based clustering revealed additional salient parameters including number of primary dendrites and dendritic segmentation which differed between clusters. Interestingly, the one cell classified as SGCs by the investigator that clustered with putative GCs was located in the IML (a feature that was not included in the cluster analysis), had a wide dendritic angle, but had more than one primary dendrite, typically seen in GCs, with complex pattern of branching which could have driven the clustering with GCs (Supplementary Figure 2D). Importantly, comparison of cell classification based on the unsupervised approach to that of the investigator (A.G.) confirmed that the investigator and PCA-based classifier agreed on the “grouping” of >85% (31 of 36) of cells examined and >96%

(26 of 27) when the cells in the mixed cluster 2 are removed. These findings confirm that GCs and SGCs are structurally distinct and demonstrate that the investigator can reliably discriminate the cell-types.

Developmental changes in somato-dendritic morphology of dentate projection neurons

Using the investigator-assigned classifications, we next examined which specific morphological parameters showed cell-type and developmental differences. First, we focused on the parameters that contributed to PCs underlying cell classification. As predicted based on the PCA, the number of primary dendrites (first order segments), second order segments and nodes were different between SGCs and GCs, with SGCs having significantly more dendritic segments in the first three orders of dendrites (Fig. 3A, Supplementary Figure 3 & Supplementary Tables 3 &4). However, the effect of *age* on the number of segments in each order was not statistically significant (Supplementary Figure 3A&B, Supplementary Tables 3 & 4). Similarly, soma width and dendritic angle were greater in SGCs and failed to show age related changes (by TW-ANOVA; Fig. 3B&C, and Supplementary Tables 3 & 4). Thus, these parameters are ideally suited to distinguish cell-types regardless of age. In contrast, dendritic length showed a significant effect of age yet was not different between cell types (Fig. 3D, and Supplementary Tables 3 & 4). Of note, SGCs had significantly lower dendritic complexity than GCs and failed to show the age-dependent increase in complexity observed in GCs (Fig. 3E, and Supplementary Tables 3 & 4). Additional parameters that reflected 3D dendritic structure including convex hull surface area showed significant differences between cell-type and with age (Fig. 3F, Supplementary Tables 3 & 4). The convex hull surface area increased with development from infancy to adolescence and remained at adolescent levels in the adult (Fig. 3F, and

Supplementary Tables 3 & 4) and appeared to contribute substantially to variability in the PCA analysis of pooled morphometric dataset (Supplementary Figure 2B). Finally, certain summed dendritic parameters including total numbers of dendritic terminals (ends), nodes, and segments showed neither cell-type nor age related differences (Supplementary Figure 3D-F, Supplementary Tables 3 & 4).

Heightened inhibitory synaptic drive to SGCs during adolescence

We previously demonstrated that SGCs from adolescent rats receive a greater frequency of action-potential driven sIPSCs than GCs from age-matched rats (Gupta A *et al.* 2012). To determine if SGC inhibitory drive changes through postnatal development, we recorded sIPSCs from SGCs and GCs in three developmental stages. As illustrated in Fig. 4, SGCs consistently showed a higher frequency of sIPSCs compared to GCs from age matched rats. Both cell-types showed changes in sIPSC frequency with age. The frequency of sIPSCs in GCs increased from infancy through adolescence, peaked at adolescence and showed a slight, yet, significant decrease in adults. (Fig. 4D, Supplementary Figure 4 and Supplementary Tables 5 & 6). Despite the decrease from adolescence to adulthood, the sIPSC frequency in GCs from adults was higher than that in infancy. SGCs, on the other hand, showed a distinct peak in sIPSC frequency during adolescence with a significant reduction in frequency in adults, back to the levels observed in infancy (Fig. 4D, Supplementary Figure 4, and Supplementary Tables 5 & 6). Thus, despite being consistently higher than in GCs, sIPSC frequency in SGCs appears to show a specific and transient enhancement during adolescence.

Unlike sIPSC frequency, SGC sIPSC amplitude did not differ from GCs in infant and adolescent rats (Fig. 5 and Supplementary Tables 5 & 6), consistent with our earlier reports in adolescent rats (Gupta A *et al.* 2012). However, GCs from adults showed a significantly larger sIPSC amplitude compared to age-matched SGCs (Fig. 5D3). In GCs, sIPSC amplitude decreased from infancy to adolescence and remained at levels similar to adolescence through adulthood (Fig. 5C). While sIPSC amplitude in SGCs decreased through postnatal development with a significant reduction from infancy to adolescence, unlike GCs, SGC sIPSC amplitude declined further in adults (Fig. 5C, Supplementary Tables 5 & 6). Since distal inhibitory inputs can attenuate to a smaller amplitude at the soma (Soltesz I et al. 1995), we sought to assess whether developmental change in GC and SGC sIPSC amplitude may be explained by changes in proximal versus distal dendritic inputs with age. To determine if there is a systematic change in the amplitude of sIPSCs with age, we assigned sIPSCs to two groups based on their amplitudes: large and putative proximal and perisomatic (>50pA), and small (<50pA), potentially dendritic. We then calculated the proportion of these events classes in GCs and SGCs during development. Consistent with the developmental increase in dendritic length and potential pruning of perisomatic events during adolescence (Tran TS et al. 2009), the proportion of large amplitude, presumed perisomatic events (>50pA) were highest in infants and reduced progressively with age while the smaller amplitude events <50pA events increased with age in both the cell types (Supplementary Figure 5). These findings indicate that developmental increase in dendritic length may contribute to decline in IPSC amplitude over age in both cell types.

Extrasynaptic GABA currents in SGCs peak during adolescence

Apart from GABAergic synaptic inputs, dentate GCs are known to express extra and perisynaptic $GABA_A$ receptors that contribute to steady-state tonic GABA currents (Stell BM et al. 2003). We previously demonstrated the presence of tonic GABA currents in SGCs and identified that the amplitude of tonic GABA current in SGCs was greater than in age-matched adolescent GCs (Gupta A *et al.* 2012). Although tonic GABA current amplitude in SGCs, measured as the baseline currents blocked by a saturating concentration of $GABA_A$ receptor antagonists, was significantly greater than in GCs during adolescence, tonic $GABA_A$ current amplitude was not different between GCs and SGCs during infancy or adulthood (Fig. 6). In GCs, the amplitude of tonic GABA current amplitude remained relatively stable through the postnatal period examined. In contrast, SGCs showed a significant increase in tonic GABA currents from infancy to adolescence which returned back to pre-adolescent levels in adults (Fig. 6 and Supplementary Tables 5 & 6) demonstrating that, SGC tonic GABA currents show a unique peak during adolescence, not observed in GCs.

Enhanced inhibitory regulation of dentate activity *in vivo* during adolescence

Transient developmental shifts in GABAergic inhibition would be expected to alter dentate output in response to input activation. Paired stimuli to the angular bundle evoked with an interval of 20ms has been reliably used to evaluate hippocampal network inhibition by local neurons, especially the basket cells (Jedlicka P et al. 2010; Jedlicka P et al. 2011). *In vivo* examination of GCL population response evoked by a pair of stimuli to the angular bundle at 20 ms interval in infant, adolescent, and adult rats identified a significant decrease in paired pulse ratios (PPR) in adolescent group compared to infant and adult groups (Fig. 7; PPR: 0.28±0.03 in n=7 adolescents vs. 0.79±0.06 in n=8 infants and 0.61±0.09 in n=6 adults; $p<0.05$, Kruskal-

Wallis one way ANOVA on ranks). In line with previous developmental studies evaluating PPR in rats (DiScenna PG and TJ Teyler 1994), we did not see a significant difference in PPR between the infants and adult groups. Thus, consistent with the increase in synaptic and tonic inhibition of dentate projection neurons, results from anesthetized rats in vivo demonstrate heightened feedback inhibitory regulation of dentate activity in response to afferent inputs during adolescence.

Discussion:

Contemporary literature on the dentate gyrus describes the projection neurons as a largely homogeneous population of GCs with limited diversity (Kesner RP 2018). Since GCs are a unique subset of neurons that undergo neurogenesis and maturation through adulthood, structural and functional diversity in GCs is largely attributed to the maturation state of neurons within the circuit (Toda T and FH Gage 2018). At any given postnatal developmental stage of the animal, immature GCs tend to be located closer the hilar border of the cell layer, have less elaborate dendritic structures and are functionally more excitable than their mature counterparts (Overstreet-Wadiche LS and GL Westbrook 2006; Kerloch T *et al.* 2018). However, emerging recognition of a distinct subset of dentate projection neurons challenges the prevailing view that dentate projection neurons are a homogenous class of cells distinguished by developmental stages (Williams PA *et al.* 2007; Gupta A *et al.* 2012; Save L *et al.* 2018). SGCs, which have been characterized in the IML of the dentate gyrus differ from GCs in their expansive dendritic arbors and show more sustained firing activity (Williams PA *et al.* 2007; Larimer P and BW Strowbridge 2010). These and other features, including their distinct window of embryonic day 12-15 for SGC development (Save L *et al.* 2018), enhanced excitatory drive (Larimer P and BW Strowbridge 2010), and distinct synaptic and extrasynaptic inhibitory currents (Gupta A *et al.* 2012) indicate that SGCs are distinct from GCs. Although SGCs have been proposed to sculpt feedback inhibition of GCs, gate dentate activity, and contribute to memory processing (Larimer P and BW Strowbridge 2010; Walker MC *et al.* 2010), there is limited information on the differences between GCs and SGCs and whether these distinct features persist through postnatal development of the animal. Our detailed and objective morphometric analysis conducted at three distinct developmental stages, namely, infant, adolescent and adult age groups demonstrates that

clustering dentate projection neurons based on somato-dendritic morphology distinguishes them into different “subtypes” corresponding to SGCs and GCs. Moreover, although the total dendritic length was not different between GCs and SGCs, SGCs consistently maintained higher synaptic inhibitory inputs than GCs demonstrating differences in inhibitory regulation. Our results demonstrate that SGCs exhibit peaks in both the frequency of synaptic inhibitory inputs and magnitude of tonic GABA currents during adolescence. In vivo analysis of paired pulse inhibition, a measure of feedback inhibition, demonstrated that dentate paired pulse inhibition was maximal during adolescence. These findings demonstrate that SGCs are a structurally and functionally distinct subtype of dentate projection neurons which is in keeping with the emerging recognition of subpopulations among hippocampal and entorhinal projection neurons (Pilli J et al. 2012; Soltesz I and A Losonczy 2018). Moreover, their uniquely heightened inhibitory regulation during adolescence suggests that SGC activity could be strongly modulated by a variety of neuroactive compounds including alcohol and neurosteroids, which selectively augment extrasynaptic GABA currents (Mody I et al. 2007; Maguire J and I Mody 2009), during adolescence.

In addition to using unbiased approaches to classify SGCs as a distinct neuronal class, our data identify key age-invariant features to distinguish the SGCs from GCs. We find that the number of primary dendrites, dendritic angle, and soma ratio are significantly higher in SGCs and can be used to categorize SGCs and GCs. In particular, the multiple primary dendrites observed in SGCs stands in stark contrast to the typical one to two apical dendrites observed in granule cell reconstructions (Thind KK et al. 2008). Indeed, the striking >85% correspondence between the unsupervised clustering and investigator assigned clustering likely stems from the investigator’s use of dendritic angle, soma width, which are significant contributors to the firsc PC, in addition

to soma location to classify cell types. Dendritic length, on the other hand, increased during development but was not different between cell types indicating that processes reflecting developmental maturation are common to the cell types. Consistent with the presence of larger dendritic angle, the convex hull 3D volume and 3D surface area of SGCs were greater than that of GCs. However, there was also a developmental increase in these parameters from infancy to adolescence and a further stabilization into adulthood in both cell types, likely reflecting the developmental increase in hippocampal volume. Interestingly, although the number of terminal nodes was not different, the dendritic complexity was significantly lower in SGCs than in GCs demonstrating differences in branching patterns. Difference in branching patterns including dendritic complexity can impact neuronal firing and intracellular signaling, as has been demonstrated in modeling studies (van Elburg RA and A van Ooyen 2010; van der Velden L et al. 2012; Li L et al. 2015). Whether dendritic morphology can account for differences in intrinsic physiology between the dentate projection neuron types (Williams PA *et al.* 2007; Gupta A *et al.* 2012; Save L *et al.* 2018) remains to be examined. The other aspect where distinguishing cell type based on morphology becomes critical is in disease. Dentate granule cells are known to undergo changes in dendritic structure including alterations in complexity under physiological conditions and in trauma and neurodegenerative diseases (Redila VA and BR Christie 2006; Llorens-Martin M *et al.* 2015; Villasana LE et al. 2015). The ability to distinguish GCs and SGCs would be crucial to quantifying and interpreting changes in morphology in trauma, epilepsy and neurodegenerative disease.

While there are clear differences in the structure, SGCs and GCs share several characteristics. Both SGCs and GCs are projection neurons, with dendrites in the dentate molecular layer and axons projecting to hippocampal CA3 (Williams PA *et al.* 2007; Gupta A *et al.* 2012; Save L *et*

al. 2018). Several dendritic parameters including total numbers of dendritic segments, nodes, terminals and dendritic tortuosity (Supplementary Table 3) showed neither cell type nor age-related differences. Similarly, SGCs, like GCs, have dendritic spines which can aid in distinguishing them from inhibitory neurons. Additionally, hilar axon collaterals of SGCs have "mossy fiber boutons" typically attributed to GCs (Supplementary Fig. 1 and Save L *et al*. 2018). Notably, in pilot clustering analysis which included a few molecular layer inhibitory neurons, the interneurons clustered on a different branch of the dendrogram than SGCs and GCs (data not shown). The similarities between GCs and SGCs are not surprising, since we previously identified that SGCs express the prospero homeobox protein 1 (Prox1) present in GCs indicating a shared lineage (Gupta A *et al.* 2012). This shared lineage was confirmed by a recent study which identified a narrow developmental window of embryonic day 12-15 during which SGCs are produced from the same precursor niche as GCs (Save L *et al.* 2018). Yet, the morphology of embryonically labeled SGCs were distinct from that of GCs labeled on the same day (Save L *et al*. 2018), demonstrating that they are a distinct population of cells rather than a cohort of GCs with a different maturation state. In this context, studies examining dendritic properties of GCs with somata located in the outer third of the molecular layer have consistently reported wider dendritic fields and distinct dendritic arbors consistent with the possibility that the outer third of the granule cell layer may consist of a mixed population of GCs and SGCs (Green EJ and JM Juraska 1985; Sun GJ et al. 2013; Kerloch T *et al.* 2018). Whether specific genetic, molecular or developmental cues guide the development of SGCs during neurogenesis or whether local molecular and spatial factors in the dentate GCL-molecular layer border contribute to elaboration of distinct dendritic arbors remains to be determined (Lefebvre JL et al. 2015; Hatami M et al. 2018). Although the mechanisms underlying specification of SGCs as a distinct population needs

further investigation, our objective unsupervised morphometric analysis identifies the key somato-dendritic structural features that distinguish SGCs from GCs through postnatal development.

A defining feature of the dentate gyrus is the presence of heavy inhibitory regulation (Coulter DA and GC Carlson 2007). Dentate GCs receive synaptic inhibition from a diverse population of neurons and are also under steady-state, tonic extrasynaptic inhibition (Harney SC and MV Jones 2002; Stell BM *et al.* 2003; Coulter DA and GC Carlson 2007; Ewell LA and MV Jones 2010). In an earlier study, we identified that SGCs are under stronger inhibitory regulation than GCs with higher frequency of inhibitory synaptic currents and greater amplitude of tonic GABA currents (Gupta A *et al.* 2012). Here, we find that SGCs continue to receive greater spontaneous synaptic inhibitory events than GCs through postnatal development. This contrasts with the lack of difference in inhibitory current between embryonically-born and adult-born mature granule cells (Laplagne DA et al. 2007). Interestingly, we find that the frequency of sIPSCs peak during adolescence in both cell types while the amplitude decreases progressively with development. Can dendritic structural features explain the cell-type specific and developmental differences in sIPSC parameters in dentate projection neurons? The consistently higher sIPSC frequency in SGCs is surprising as the dendritic lengths and location are not different between GCs and SGCs (Fig. 3). The wider dendritic distribution of SGCs, also reflected in the greater convex hull 3D volume, could allow for inputs from a larger group of inhibitory neurons to impinge on SGC dendrites, while GCs with their compact dendritic distribution may receive fewer inputs. It is also possible that the relatively early embryonic development of SGCs increases the chance of SGCs to receive more synaptic inputs compared to GCs which develop later into adulthood. However, since both dendritic length and convex hull 3D volume increase with postnatal

development of both cells, changes in dendritic morphology or embryonic development are unlikely to account for the peak in sIPSC frequency in adolescence followed by decline in adults. Rather, developmental increase in synapses from infancy to adolescence followed by pruning or synapse elimination into adulthood (Tran TS *et al.* 2009; Riccomagno MM and AL Kolodkin 2015) could account for a peak in synaptic inhibition during adolescence. The progressive decrease in sIPSC amplitude with development in both SGCs and GCs could reflect the increase in dendritic length with development which would be expected to contribute to more distal synapses with greater dendritic attenuation or selective pruning of proximal inputs (Tran TS *et al.* 2009). Consistent with this proposal, the proportion of large amplitude events decrease progressively with development in both cell types (Supplementary Figure 5). Functionally, this enhanced synaptic inhibitory tone during adolescence is reflected in the greater paired pulse inhibition of dentate afferent-evoked responses *in vivo*. It would be important for future studies to ascertain how the differences in basal synaptic inhibition impact the recruitment and circuit function of SGCs and GCs during network activity and with development. Since basal inhibition in the dentate gyrus regulates synaptic plasticity and pattern separation at the level of the circuit (Dengler CG and DA Coulter 2016; Madar AD et al. 2019), and SGCs have been proposed to contribute to dentate pattern separation (Larimer P and BW Strowbridge 2010), developmental changes in GC and SGC inhibition are likely to influence memory and cognitive performance.

In parallel, the amplitude of extrasynaptic GABA currents in SGCs also peaked during adolescence. Although the GC data showed a trend suggesting a peak during adolescence, statistically rigorous analysis considering multiple groups was unable to reveal the developmental changes in GC tonic GABA currents quantified in previous studies (Holter NI *et al.* 2010). However, pairwise t-tests of GC tonic GABA current amplitude at different

developmental stages, similar to the analysis in Holter NI *et al.* (2010), suggested an increase in GC tonic GABA currents from infancy to adolescence and a subsequent decrease into adulthood (data not shown). Increase in expression of the extrasynaptic $GABA_AR$ δ subunit in both GCs and SGCs (Maguire J and I Mody 2009; Gupta A *et al.* 2012) is likely to mediate the increases in tonic GABA currents from infancy to adolescence. Additionally, changes in synaptically released GABA accompanying changes in sIPSCs frequency, reported here, could contribute to the peak in extrasynaptic GABA exhibited in adolescence. An interesting feature of tonic GABA currents mediated by $GABA_AR$ δ subunit is their robust enhancement by neurosteroids, raising the possibility that increases in ambient neurosteroids during adolescence (Harden C and NJ MacLusky 2004; Maguire J and I Mody 2009) could augment tonic GABA currents. Since tonic GABA currents mediated by $GABA_AR$ δ subunits are exquisitely sensitive to ethanol (Mody I *et al.* 2007), the greater magnitude of tonic GABA currents in SGCs during adolescence is likely to render SGCs vulnerable to ethanol modulation and impact their role in dentate processing. Indeed, behavioral deficits following alcohol administration have been shown to be particularly accentuated during adolescence (Spanos M et al. 2012; Lacaille H et al. 2015).

Together, the structural and functional data identify SGCs as a cell type which differs from GCs in somato-dendritic structure and developmental plasticity of steady state inhibition. Our data demonstrate that SGCs have uniquely heightened inhibitory regulation during adolescence which suggests that they may be subject to extensive endogenous and exogenous modulation of activity levels during adolescence. Notably, our results delineate salient structural features that enable anatomical identification of this subpopulation of dentate projection neurons. The novel data defining the structural features of SGCs will allow for future targeted analysis of their molecular profile and microcircuit connectivity to better understand their role in circuit function and

behaviors. In conclusion, the fundamental characterization of SGCs presented here will support incorporation of SGCs into current models of the dentate gyrus and consideration of their role in dentate microcircuit processing in health and disease.

Acknowledgements

We thank Dr. Luke Fritzky at the Rutgers Imaging Core for help with imaging and Dipika Sekhar for data entry. We thank Dr. Kelly A. Hamilton for thoughtful discussions and comments. The project was supported by National Institutes of Health/National Institute of Neurological Diseases and Stroke R01 NS069861, R01NS097750 and NJCBIR CBIR16IRG017 to V.S. and, NJCBIR CBIR11FEL003 to A.G.

Reference List

Coulter DA, Carlson GC. 2007. Functional regulation of the dentate gyrus by GABA-mediated inhibition. ProgBrain Res. 163:235-243.

Dengler CG, Coulter DA. 2016. Normal and epilepsy-associated pathologic function of the dentate gyrus. Prog Brain Res. 226:155-178.

Dieni CV, Chancey JH, Overstreet-Wadiche LS. 2012. Dynamic functions of GABA signaling during granule cell maturation. Front Neural Circuits. 6:113.

DiScenna PG, Teyler TJ. 1994. Development of inhibitory and excitatory synaptic transmission in the rat dentate gyrus. Hippocampus. 4:569-576.

Duffy CJ, Rakic P. 1983. Differentiation of granule cell dendrites in the dentate gyrus of the rhesus monkey: a quantitative Golgi study. J Comp Neurol. 214:224-237.

Engel D, Jonas P. 2005. Presynaptic action potential amplification by voltage-gated Na+ channels in hippocampal mossy fiber boutons. Neuron. 45:405-417.

Ewell LA, Jones MV. 2010. Frequency-tuned distribution of inhibition in the dentate gyrus. The Journal of neuroscience : the official journal of the Society for Neuroscience. 30:12597-12607.

Freiman TM, Eismann-Schweimler J, Frotscher M. 2011. Granule cell dispersion in temporal lobe epilepsy is associated with changes in dendritic orientation and spine distribution. Exp Neurol. 229:332-338.

Green EJ, Juraska JM. 1985. The dendritic morphology of hippocampal dentate granule cells varies with their position in the granule cell layer: a quantitative Golgi study. Exp Brain Res. 59:582-586.

Gupta A, Elgammal FS, Proddutur A, Shah S, Santhakumar V. 2012. Decrease in tonic inhibition contributes to increase in dentate semilunar granule cell excitability after brain injury. J Neurosci. 32:2523-2537.

Harden C, MacLusky NJ. 2004. Aromatase inhibition, testosterone, and seizures. Epilepsy Behav. 5:260-263.

Harney SC, Jones MV. 2002. Pre- and postsynaptic properties of somatic and dendritic inhibition in dentate gyrus. Neuropharmacology. 43:584-594.

Hatami M, Conrad S, Naghsh P, Alvarez-Bolado G, Skutella T. 2018. Cell-Biological Requirements for the Generation of Dentate Gyrus Granule Neurons. Front Cell Neurosci. 12:402.

Hollrigel GS, Ross ST, Soltesz I. 1998. Temporal patterns and depolarizing actions of spontaneous GABAA receptor activation in granule cells of the early postnatal dentate gyrus. J Neurophysiol. 80:2340-2351.

Holter NI, Zylla MM, Zuber N, Bruehl C, Draguhn A. 2010. Tonic GABAergic control of mouse dentate granule cells during postnatal development. Eur J Neurosci. 32:1300-1309.

Husson F, Josse J, Pages J. 2010. Principal component methods - hierarchical clustering - partitional clustering: why would we need to choose for visualizing data? In. Technical Report – Agrocampus.

Jedlicka P, Deller T, Schwarzacher SW. 2010. Computational modeling of GABAA receptor-mediated paired-pulse inhibition in the dentate gyrus. J Comput Neurosci. 29:509-519.

Jedlicka P, Hoon M, Papadopoulos T, Vlachos A, Winkels R, Poulopoulos A, Betz H, Deller T, Brose N, Varoqueaux F, Schwarzacher SW. 2011. Increased dentate gyrus excitability in neuroligin-2-deficient mice in vivo. Cereb Cortex. 21:357-367.

Kerloch T, Clavreul S, Goron A, Abrous DN, Pacary E. 2018. Dentate Granule Neurons Generated During Perinatal Life Display Distinct Morphological Features Compared With Later-Born Neurons in the Mouse Hippocampus. Cereb Cortex.

Kesner RP. 2018. An analysis of dentate gyrus function (an update). Behav Brain Res. 354:84-91.

Lacaille H, Duterte-Boucher D, Liot D, Vaudry H, Naassila M, Vaudry D. 2015. Comparison of the deleterious effects of binge drinking-like alcohol exposure in adolescent and adult mice. J Neurochem. 132:629-641.

Laplagne DA, Kamienkowski JE, Esposito MS, Piatti VC, Zhao C, Gage FH, Schinder AF. 2007. Similar GABAergic inputs in dentate granule cells born during embryonic and adult neurogenesis. Eur J Neurosci. 25:2973-2981.

Larimer P, Strowbridge BW. 2010. Representing information in cell assemblies: persistent activity mediated by semilunar granule cells. Nat Neurosci. 13:213-222.

Lee CY, Liou HH. 2013. GABAergic tonic inhibition is regulated by developmental age and epilepsy in the dentate gyrus. Neuroreport. 24:515-519.

Lefebvre JL, Sanes JR, Kay JN. 2015. Development of dendritic form and function. Annu Rev Cell Dev Biol. 31:741-777.

Li L, Gervasi N, Girault JA. 2015. Dendritic geometry shapes neuronal cAMP signalling to the nucleus. Nat Commun. 6:6319.

Li Y, Aimone JB, Xu X, Callaway EM, Gage FH. 2012. Development of GABAergic inputs controls the contribution of maturing neurons to the adult hippocampal network. Proc Natl Acad Sci U S A. 109:4290-4295.

Llorens-Martin M, Rabano A, Avila J. 2015. The Ever-Changing Morphology of Hippocampal Granule Neurons in Physiology and Pathology. Front Neurosci. 9:526.

Madar AD, Ewell LA, Jones MV. 2019. Temporal pattern separation in hippocampal neurons through multiplexed neural codes. PLoS Comput Biol. 15:e1006932.

Maguire J, Mody I. 2009. Steroid hormone fluctuations and GABA(A)R plasticity. Psychoneuroendocrinology. 34 Suppl 1:S84-90.

Mody I, Glykys J, Wei W. 2007. A new meaning for "Gin & Tonic": tonic inhibition as the target for ethanol action in the brain. Alcohol. 41:145-153.

Neuberger EJ, Swietek B, Corrubia L, Prasanna A, Santhakumar V. 2017. Enhanced Dentate Neurogenesis after Brain Injury Undermines Long-Term Neurogenic Potential and Promotes Seizure Susceptibility. Stem Cell Reports. 9:972-984.

Overstreet-Wadiche LS, Westbrook GL. 2006. Functional maturation of adult-generated granule cells. Hippocampus. 16:208-215.

Pilli J, Abbasi S, Richardson M, Kumar SS. 2012. Diversity and excitability of deep-layer entorhinal cortical neurons in a model of temporal lobe epilepsy. J Neurophysiol. 108:1724-1738.

Ramón y Cajal S. 1953. Histologie du système nerveux de l'homme & des vertébrés. Madrid,: Consejo Superior de Investigaciones Científicas, Instituto Ramón y Cajal.

Redila VA, Christie BR. 2006. Exercise-induced changes in dendritic structure and complexity in the adult hippocampal dentate gyrus. Neuroscience. 137:1299-1307.

Riccomagno MM, Kolodkin AL. 2015. Sculpting neural circuits by axon and dendrite pruning. Annu Rev Cell Dev Biol. 31:779-805.

Sancho-Bielsa FJ, Navarro-Lopez JD, Alonso-Llosa G, Molowny A, Ponsoda X, Yajeya J, Lopez-Garcia C. 2012. Neurons of the dentate molecular layer in the rabbit hippocampus. PLoS One. 7:e48470.

Save L, Baude A, Cossart R. 2018. Temporal Embryonic Origin Critically Determines Cellular Physiology in the Dentate Gyrus. Cereb Cortex.

Semple BD, Blomgren K, Gimlin K, Ferriero DM, Noble-Haeusslein LJ. 2013. Brain development in rodents and humans: Identifying benchmarks of maturation and vulnerability to injury across species. Prog Neurobiol. 106-107:1-16.

Sengupta P. 2013. The Laboratory Rat: Relating Its Age With Human's. Int J Prev Med. 4:624-630.

Seress L, Frotscher M. 1990. Morphological variability is a characteristic feature of granule cells in the primate fascia dentata: a combined Golgi/electron microscope study. J Comp Neurol. 293:253-267.

Soltesz I, Losonczy A. 2018. CA1 pyramidal cell diversity enabling parallel information processing in the hippocampus. Nat Neurosci. 21:484-493.

Soltesz I, Smetters DK, Mody I. 1995. Tonic inhibition originates from synapses close to the soma. Neuron. 14:1273-1283.

Spanos M, Besheer J, Hodge CW. 2012. Increased sensitivity to alcohol induced changes in ERK Map kinase phosphorylation and memory disruption in adolescent as compared to adult C57BL/6J mice. Behav Brain Res. 230:158-166.

Stell BM, Brickley SG, Tang CY, Farrant M, Mody I. 2003. Neuroactive steroids reduce neuronal excitability by selectively enhancing tonic inhibition mediated by delta subunit-containing GABAA receptors. Proc Natl Acad Sci U S A. 100:14439-14444.

Sun GJ, Sailor KA, Mahmood QA, Chavali N, Christian KM, Song H, Ming GL. 2013. Seamless reconstruction of intact adult-born neurons by serial end-block imaging reveals complex axonal guidance and development in the adult hippocampus. J Neurosci. 33:11400-11411.

Swietek B, Gupta A, Proddutur A, Santhakumar V. 2016. Immunostaining of Biocytin-filled and Processed Sections for Neurochemical Markers. J Vis Exp.

Thind KK, Ribak CE, Buckmaster PS. 2008. Synaptic input to dentate granule cell basal dendrites in a rat model of temporal lobe epilepsy. J Comp Neurol. 509:190-202.

Toda T, Gage FH. 2018. Review: adult neurogenesis contributes to hippocampal plasticity. Cell Tissue Res. 373:693-709.

Tran TS, Rubio ME, Clem RL, Johnson D, Case L, Tessier-Lavigne M, Huganir RL, Ginty DD, Kolodkin AL. 2009. Secreted semaphorins control spine distribution and morphogenesis in the postnatal CNS. Nature. 462:1065-1069.

van der Velden L, van Hooft JA, Chameau P. 2012. Altered dendritic complexity affects firing properties of cortical layer 2/3 pyramidal neurons in mice lacking the 5-HT3A receptor. J Neurophysiol. 108:1521-1528.

van Elburg RA, van Ooyen A. 2010. Impact of dendritic size and dendritic topology on burst firing in pyramidal cells. PLoS Comput Biol. 6:e1000781.

Villasana LE, Kim KN, Westbrook GL, Schnell E. 2015. Functional Integration of Adult-Born Hippocampal Neurons after Traumatic Brain Injury(1,2,3). eNeuro. 2.

von Campe G, Spencer DD, de Lanerolle NC. 1997. Morphology of dentate granule cells in the human epileptogenic hippocampus. Hippocampus. 7:472-488.

Walker MC, Pavlov I, Kullmann DM. 2010. A 'sustain pedal' in the hippocampus? Nature neuroscience. 13:146-148.

Williams PA, Larimer P, Gao Y, Strowbridge BW. 2007. Semilunar granule cells: glutamatergic neurons in the rat dentate gyrus with axon collaterals in the inner molecular layer. J Neurosci. 27:13756-13761.

Yu EP, Dengler CG, Frausto SF, Putt ME, Yue C, Takano H, Coulter DA. 2013. Protracted postnatal development of sparse, specific dentate granule cell activation in the mouse hippocampus. J Neurosci. 33:2947-2960.

Yu J, Proddutur A, Elgammal FS, Ito T, Santhakumar V. 2013. Status epilepticus enhances tonic GABA currents and depolarizes GABA reversal potential in dentate fast-spiking basket cells. J Neurophysiol. 109:1746-1763.

Yu J, Proddutur A, Swietek B, Elgammal FS, Santhakumar V. 2016. Functional Reduction in Cannabinoid-Sensitive Heterotypic Inhibition of Dentate Basket Cells in Epilepsy: Impact on Network Rhythms. Cereb Cortex. 26:4229-4314.

Figure Legends

Figure 1. Somato-dendritic differences in dentate projection neurons - GCs and SGCs. Representative neuronal reconstructions of GC (1A-F) and SGC (1G-L) showing distinct dendritic arbors from infant (top), adolescent (middle) and adult (bottom) age groups. Note that images are shown in different planes for each age group. The complexity of dendrites is shown in XY planes for GCs and SGCs 'A, B, C' and 'G, H, I' respectively and perpendicular view is shown in 'D, E, F' for GCs and 'J, K, L' for SGCs. Inset images in the center represent the color coding for dendritic segments from proximal to distal axes. Scale bar: 100µm.

Figure 2. Hierarchical clustering on principal component reveals two major clusters of dentate projection neurons. (A-B) 3D representation of the principle component analysis of individuals resolved by first three principle components, with confidence interval (CI) ellipsoid set to 0.95. The plot suggests grouping by cell type (A) but not by age (B). (C) Hierarchical clustering on Principal Components based on 42 morphometric parameters (Supplementary Tables 1 & 2) was performed using Ward's method with Euclidean distance to generate the dendrogram. Dendrogram classifies neurons into two major groups which resolved into 4 putative clusters. Cells in which the classifier and experimenter failed to concur on classification are represented by green arrowheads based on investigator assigned classification.

Figure 3: Comparison of morphometric parameters between GCs and SGCs at distinct developmental stages. Summary plots of averages no. of primary dendrites (A), soma width (B), dendritic angle (C), total dendritic length (D), dendritic complexity (E), and convex hull surface area (F) of GCs and SGCs at three developmental time points. *, #, and $ denote $p<0.05$ for

differences between cell types, in GC across age groups and SGC across age groups, respectively by TW-ANOVA followed by post-hoc pairwise comparison (Supplementary Tables 3 & 4).

Figure 4: Developmental differences in sIPSC frequencies of GCs and SGCs. Representative sIPSC traces in GCs (left, A1, B1, C1) and SGCs (right, A2, B2, C2) in infant, adolescent, and adult age groups. Summary plot of developmental differences in sIPSC frequency between and within GCs and SGCs (D). *, #, and $ denote $p<0.05$ for differences between cell types, in GC across age groups and SGC across age groups, respectively by TW-ANOVA followed by post-hoc pairwise comparison (Supplementary Tables 5 & 6). Cumulative probability plots of sIPSCs frequency showing significant between cell types differences at infant (E1), adolescent (E2) and adult (E3) age groups * denotes $p<0.05$ for differences between cell types by Kruskal-Wallis Test (Supplementary Tables 5 & 6).

Figure 5: Developmental changes in sIPSC amplitudes of GCs and SGCs. Overly of representative average sIPSC waveforms from GCs (A) and SGCs (B) in different age groups. Summary plot of sIPSC amplitude at the three developmental stages in both cell types (C). *, #, and $ denote $p<0.05$ for differences between cell types, in GC across age groups and SGC across age groups, respectively by TW-ANOVA followed by post-hoc pairwise comparison (Supplementary Tables 5 & 6). Cumulative probability plots of sIPSC amplitudes of infant (D1), adolescent (D2) and adult (D3) age groups. * denotes $p<0.05$ for differences between cell types by Kruskal-Wallis Test (Supplementary Tables 5 & 6).

Figure 6: Extrasynaptic tonic GABAergic currents in SGCs peak during adolescence. Representative baseline current recordings in GCs (left, A1-3) and SGCs (right, B1-3) in infant,

adolescent and adult age groups. Tonic GABA current is measured as the difference in baseline current upon perfusion of the GABA receptor antagonist BMI (100µM). Gaussian fit to the positive half of the baseline current, under basal conditions and in BMI, is illustrated on the right of each trace and was used to quantify tonic GABA. (C) Summary plot showing average tonic GABAergic currents at three distinct time points. *, #, and $ denote $p<0.05$ for differences between cell types and in SGC across age groups, respectively by TW-ANOVA followed by post-hoc pairwise comparison (Supplementary Tables 5 & 6).

Figure 7: Paired pulse inhibition as a measure of local feedback inhibition. (A) Shows representative traces showing paired pulse inhibition among infant, adolescent and adult groups in response to activation of medial Perforant path(mPP) in anesthetized rats. Note the difference in y scale bars. (B) Box plot showing the distribution of paired pulse ratio's between the groups (infant vs adolescent $p=<0.001$; adolescent vs adults $p=0.007$; infants vs adults $p=0.068$: * indicates $p<0.05$ by One-way ANOVA followed by pairwise comparison by Post-hoc Holm-Sidak method.

Supplementary Figure legends

Supplementary Figure 1: Representative images of a GC and SGC. Images of a typical GC (A) and SGC (B) illustrate the somatic location, dendritic arbor, with high density of spines (insets, white arrows) and axons with boutons (white arrow heads) targeting CA3 used by experimenter to classify SGCs and GCs. Scale bar: 100µm; Inset scale bar: 20 µm.

Supplementary Figure 2: Analysis of Morphological Variables underlying Principal Components. A. Histogram illustrates percentage of information retained by each dimension (principal component, PC). B. Factor maps illustrate the quality of representation of the morphometric variables measured by cos2 (square cosine, squared coordinates). The darker color indicates stronger contribution to variability to PC . C. Representation of the top five variables in the first two dimensions. D. Neuronal reconstructions of SGC in first cluster (notice higher complexity than other SGCs in figure 1). Scale bar: 100µm.

Supplementary Figure 3: Comparison of morphometric parameters between GCs and SGCs at distinct developmental stages. Summary plot of number of second (A) and third (B) order dendritic segments, second order nodes (C), total number of dendritic ends (D), total dendritic nodes (E) and total dendritic segments (F) in GCs and SGCs at the three age groups examined. * denotes $p<0.05$ for differences between cell types by TW-ANOVA followed by post-hoc pairwise comparison (Supplementary Tables 3 & 4).

Supplementary Figure 4: Cumulative plots of sIPSC frequency in GCs and SGCs through development. Cumulative plots of sIPSC frequency comparing three age groups * denotes

$p<0.05$ for differences between cell types by Kruskal-Wallis Test (Supplementary Table 6) in GCs (A) and SGCs (B).

Supplementary Figure 5: Developmental differences in distribution of sIPSC amplitudes in GCs and SGCs. Pie chart distributions illustrating subjective percentage distribution of high peak amplitude (>50pA) and smaller peak amplitude (<50 pA) amplitude sIPSCs in GCs (top) and SGCs (bottom) across age groups.

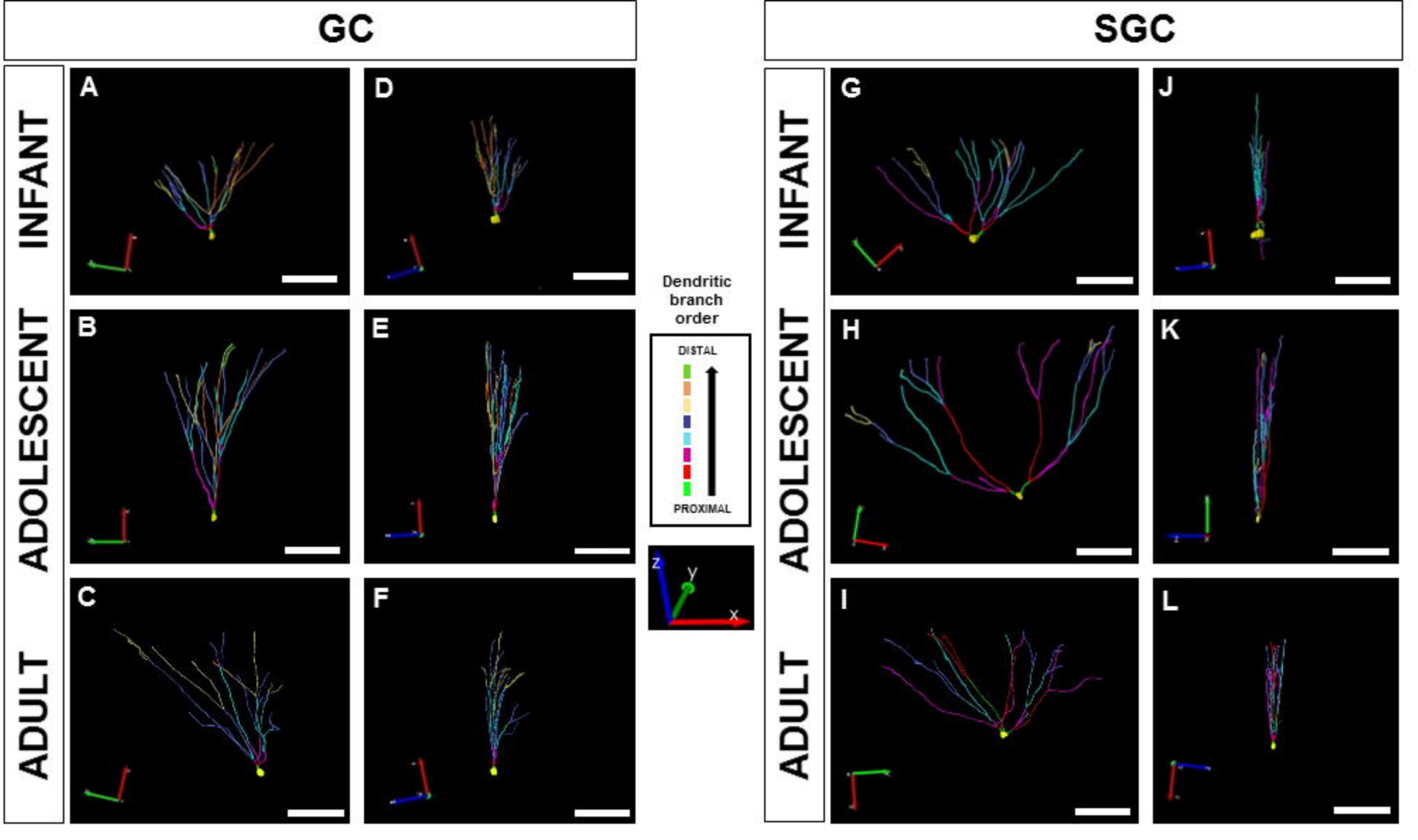
GC
SGC
INFANT
ADOLESCENT
ADULT
A
B
C
D
E
F
G
H
I
J
K
L
Dendritic branch order
DISTAL
PROXIMAL
z
y
x

Figure 2

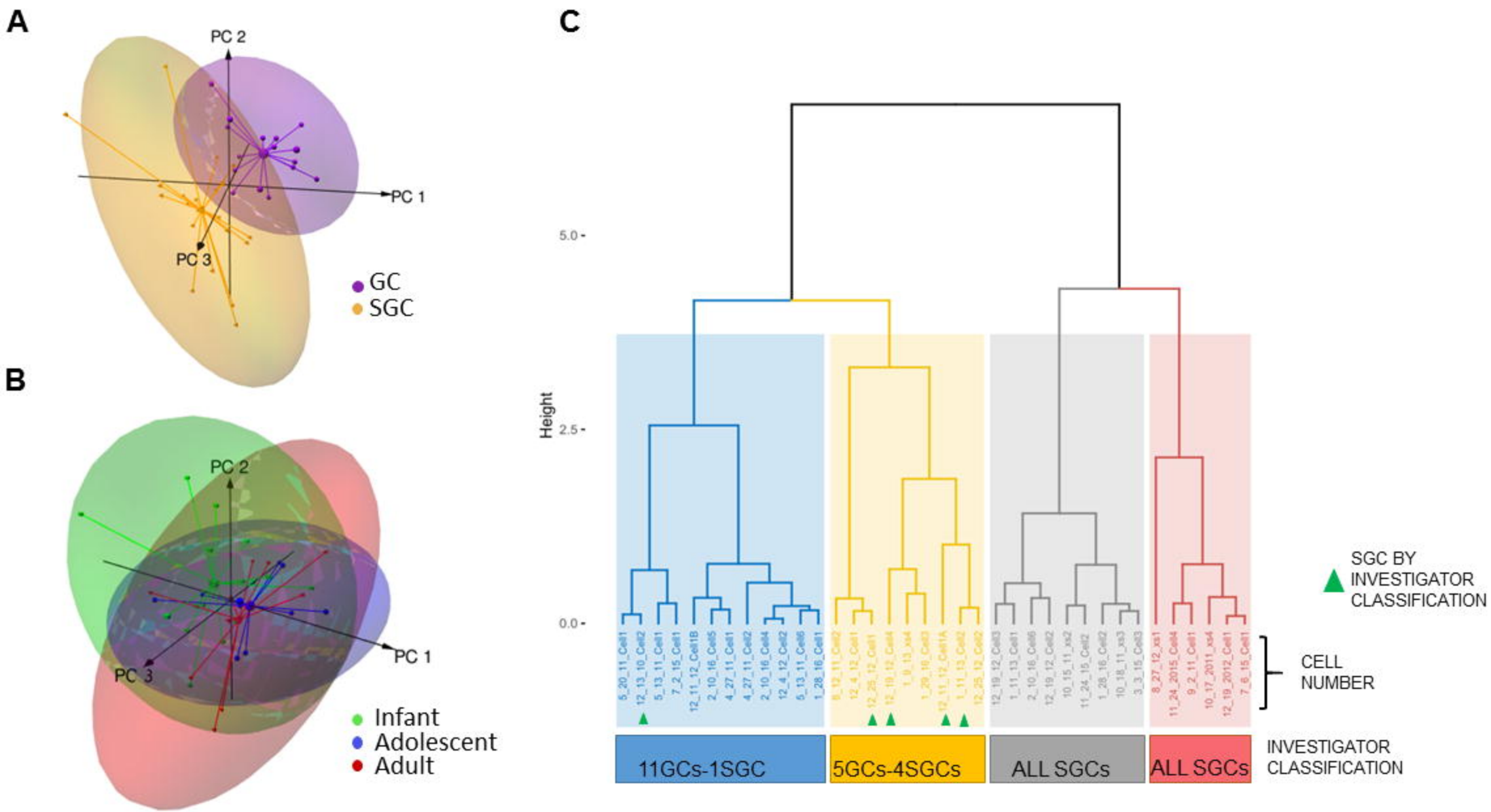
A
PC 2
PC 1
PC 3
GC
SGC
B
PC 2
PC 1
PC 3
Infant
Adolescent
Adult
C
Height
5.0
2.5
0.0
SGC BY INVESTIGATOR CLASSIFICATION
CELL NUMBER
11GCs-1SGC
5GCs-4SGCs
ALL SGCs
ALL SGCs
INVESTIGATOR CLASSIFICATION

Figure 3

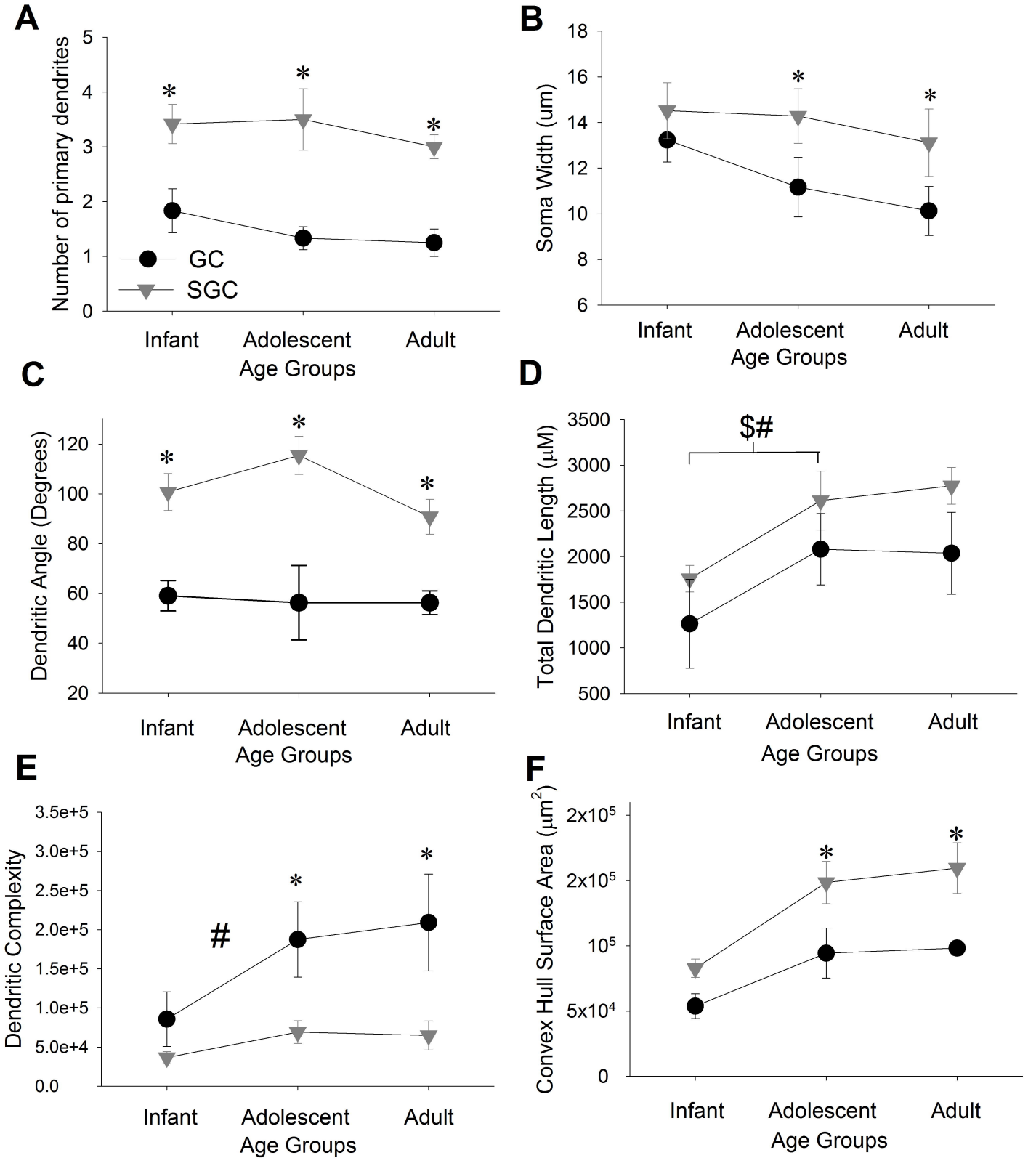
A
Number of primary dendrites
0
1
2
3
4
5
*
*
*
GC
SGC
Infant
Adolescent
Adult
Age Groups
B
Soma Width (um)
6
8
10
12
14
16
18
*
*
Infant
Adolescent
Adult
Age Groups
C
Dendritic Angle (Degrees)
20
40
60
80
100
120
*
*
*
Infant
Adolescent
Adult
Age Groups
D
Total Dendritic Length (μM)
500
1000
1500
2000
2500
3000
3500
$#
Infant
Adolescent
Adult
Age Groups
E
Dendritic Complexity
0.0
5.0e+4
1.0e+5
1.5e+5
2.0e+5
2.5e+5
3.0e+5
3.5e+5
#
*
*
Infant
Adolescent
Adult
Age Groups
F
Convex Hull Surface Area (μm2)
0
5x10^4
10^5
2x10^5
2x10^5
*
*
Infant
Adolescent
Adult
Age Groups

Figure 4

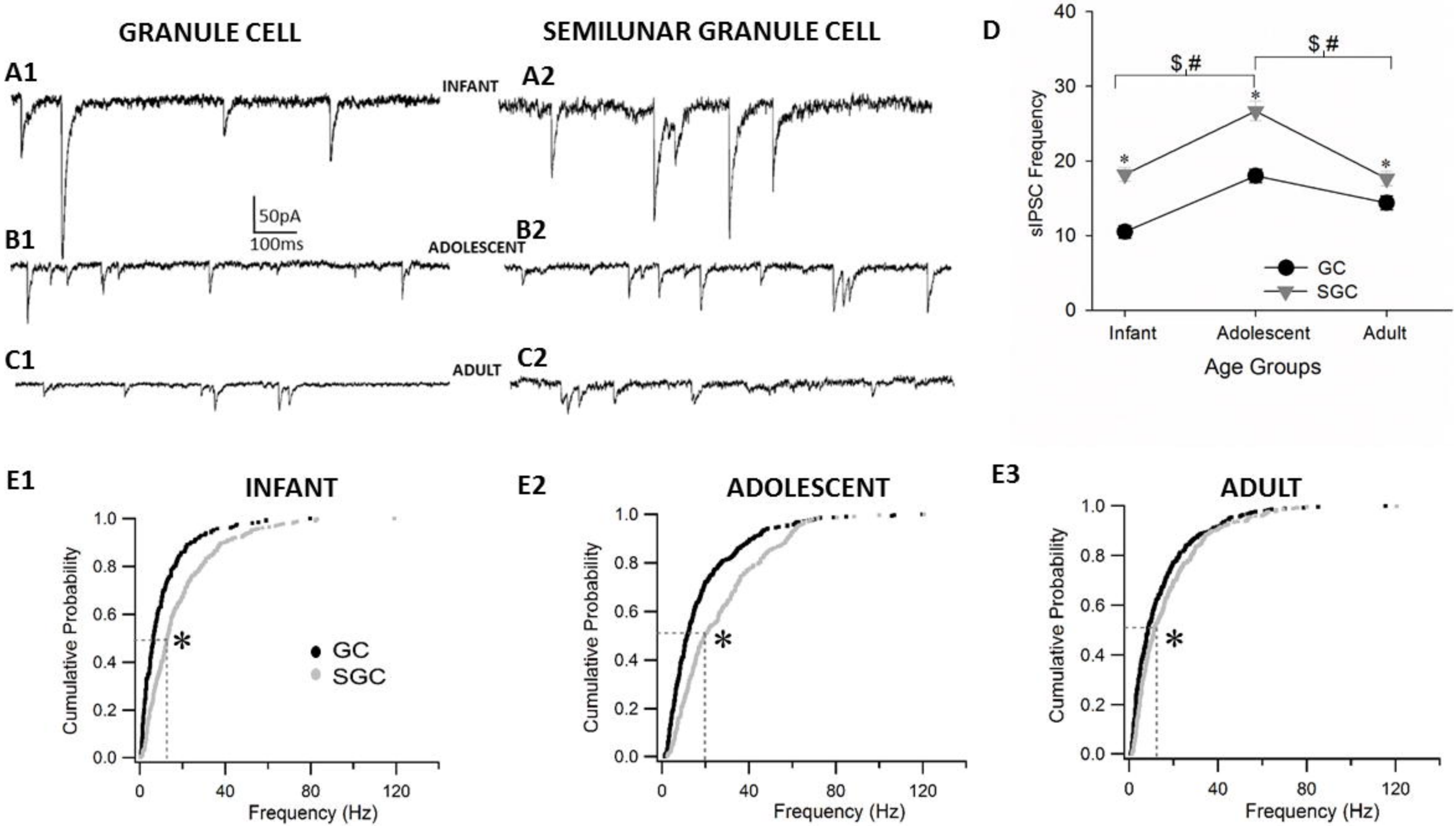
GRANULE CELL
SEMILUNAR GRANULE CELL
A1
A2
INFANT
B1
B2
ADOLESCENT
C1
C2
ADULT
50pA
100ms
D
sIPSC Frequency
Age Groups
Infant
Adolescent
Adult
GC
SGC
$ #
E1
E2
E3
INFANT
ADOLESCENT
ADULT
Cumulative Probability
Frequency (Hz)
GC
SGC

Figure 5

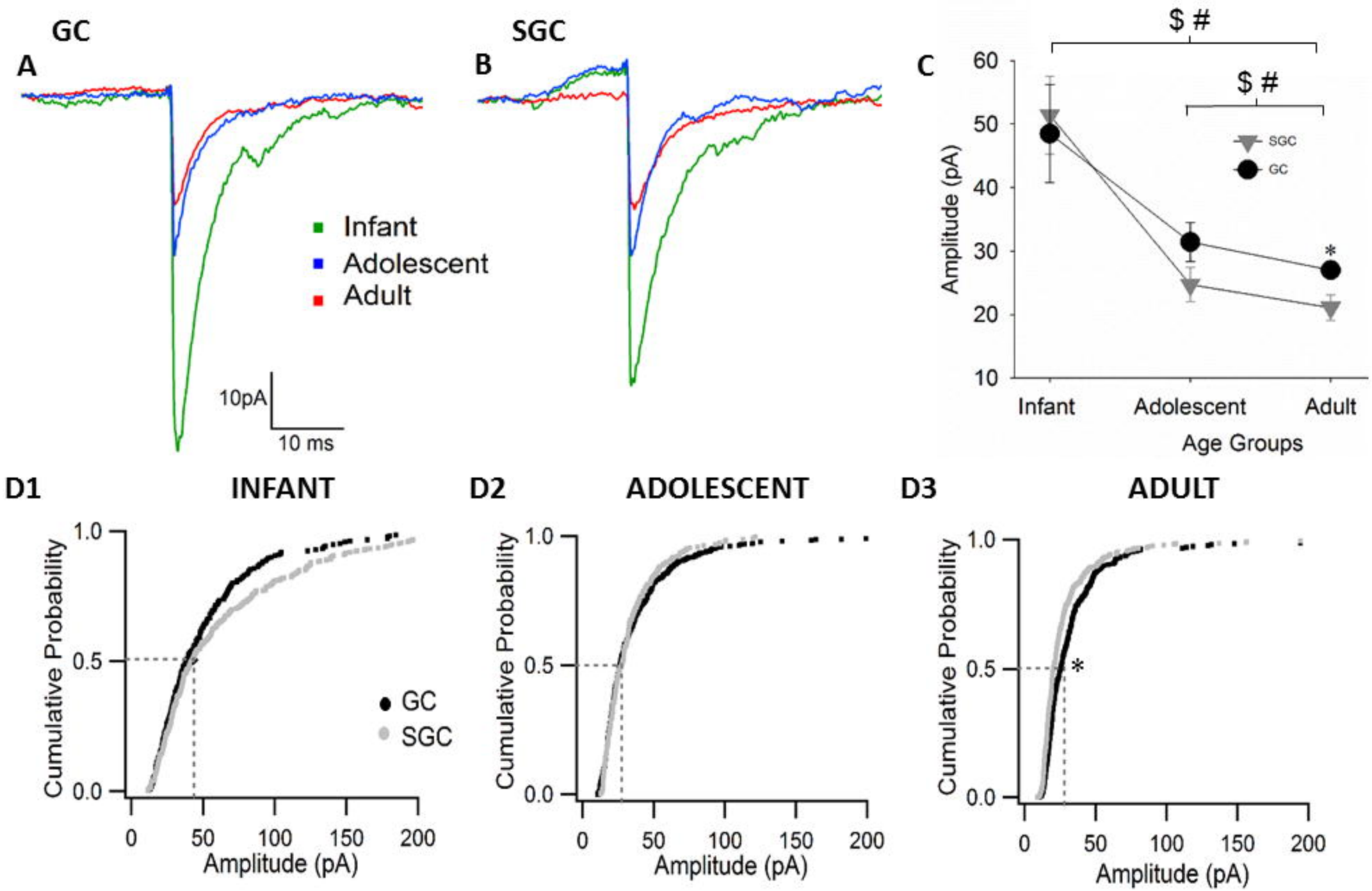
GC
A
Infant
Adolescent
Adult
10pA
10 ms
SGC
B
C
$ #
$ #
SGC
GC
Amplitude (pA)
Infant
Adolescent
Adult
Age Groups
D1
INFANT
D2
ADOLESCENT
D3
ADULT
Cumulative Probability
GC
SGC
Amplitude (pA)

Figure 6

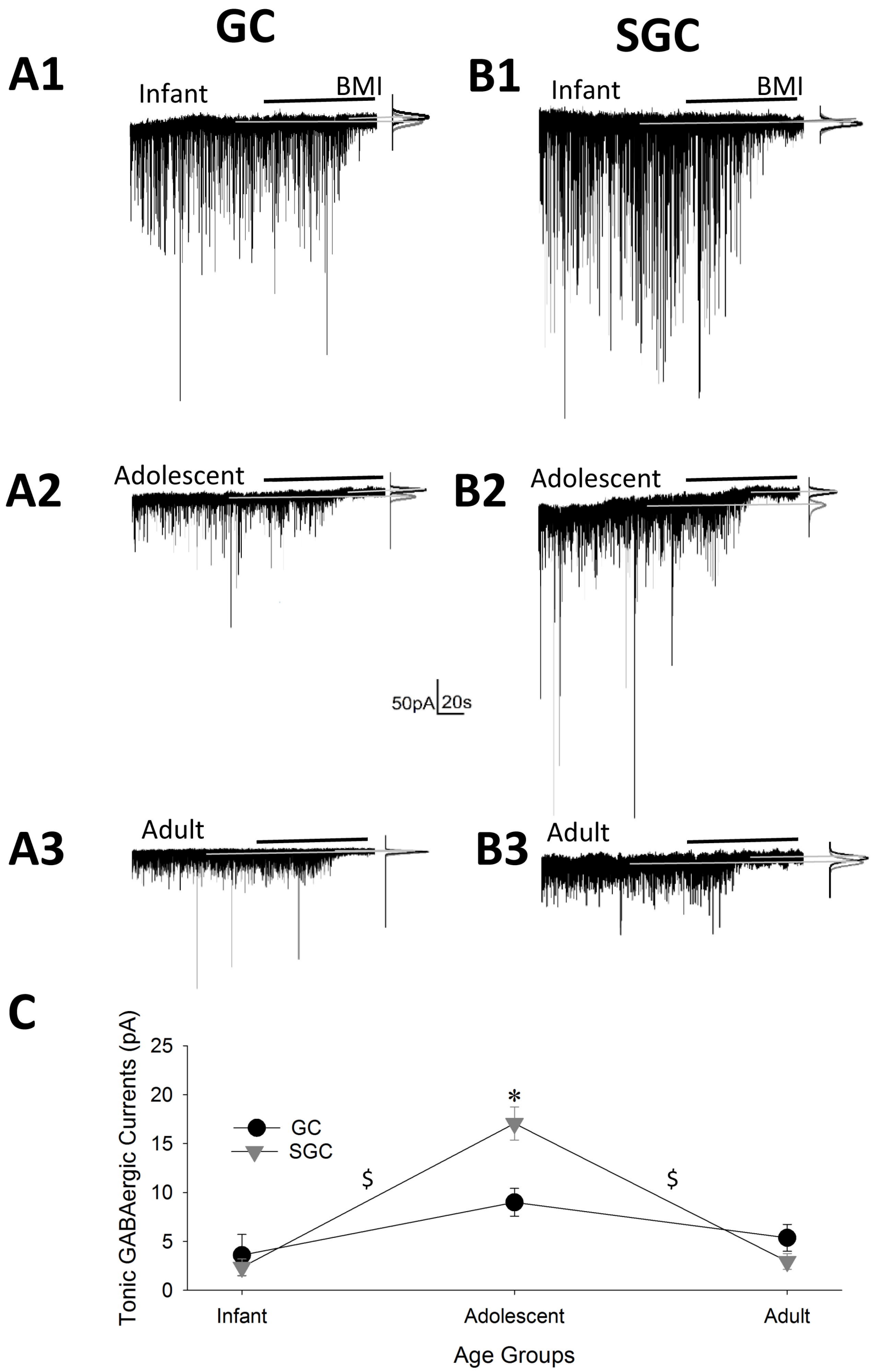
GC
SGC
A1
B1
Infant
BMI
Infant
BMI
A2
Adolescent
B2
Adolescent
50pA
20s
A3
Adult
B3
Adult
C
Tonic GABAergic Currents (pA)
25
20
15
10
5
0
GC
SGC
*
$
$
Infant
Adolescent
Adult
Age Groups

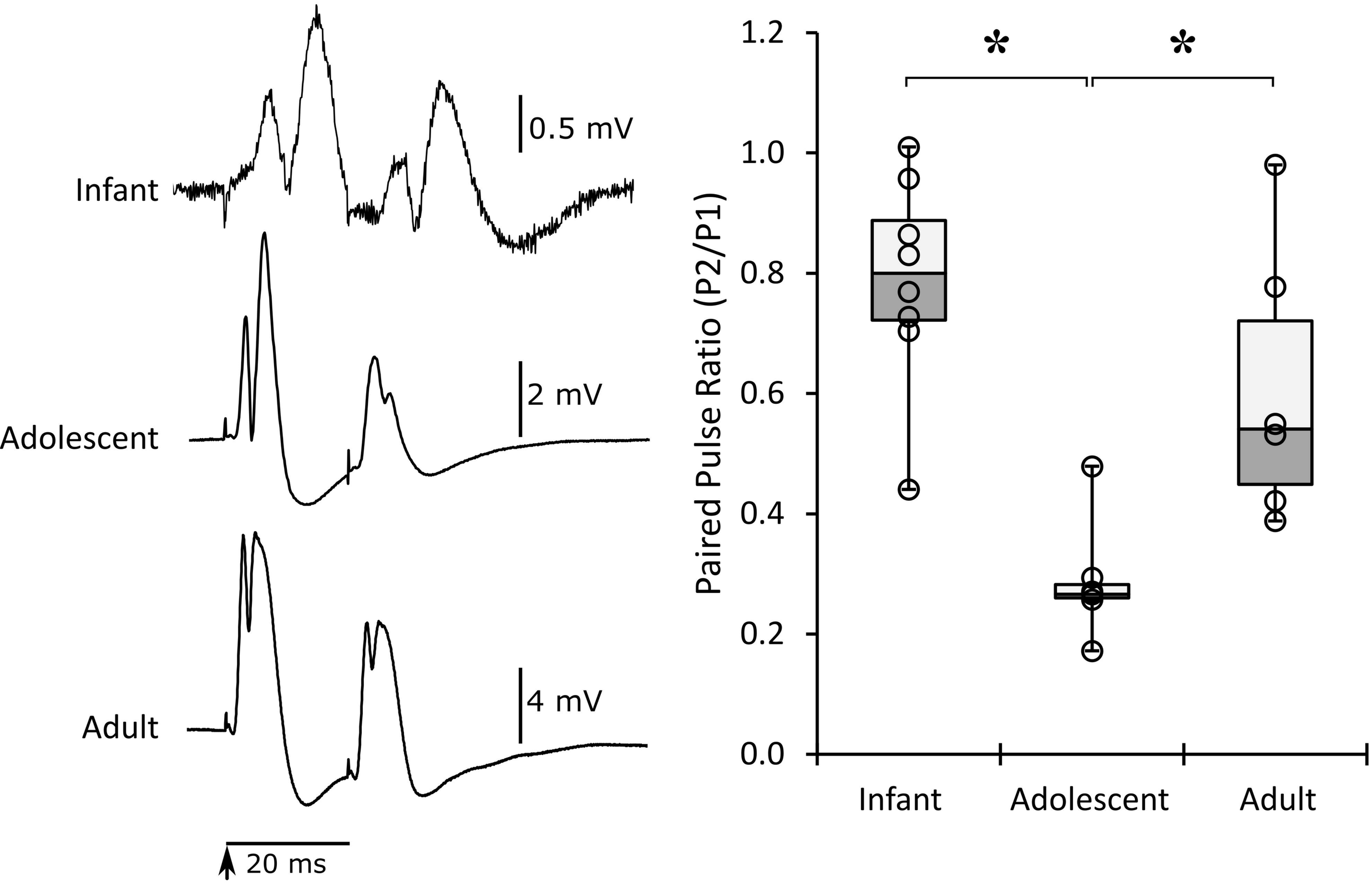
Infant
0.5 mV
Adolescent
2 mV
Adult
4 mV
20 ms
Paired Pulse Ratio (P2/P1)
1.2
1.0
0.8
0.6
0.4
0.2
0.0
*
*
Infant
Adolescent
Adult